Uncertainty analysis of band gaps for beams with periodically distributed resonators produced by additive manufacturing

A. T. Fabro[1], D. Beli[2], J. R. F. Arruda[2], N. S. Ferguson[3], B. R. Mace[4]
[1] Department of Mechanical Engineering, University of Brasilia, Brasilia-DF, Brazil
e-mail: **fabro@unb.br**

[2] Department of Computation Mechanics, University of Campinas, Campinas-SP, Brazil

[3] ISVR, University of Southampton, Southampton, UK

[4] Department of Mechanical Engineering, University of Auckland, Auckland, New Zealand

Abstract
Periodic structures can be designed to exhibit elastic band gap behaviour by varying material or geometrical properties, i.e. phononic crystals, or by periodically distributed resonators or boundary conditions, i.e. acoustic metamaterials, with various applications in passive noise and vibration control. The additive manufacturing, or 3D printing, has been used in the production of structures with complex features at low cost and, even though it can significantly affect the band gap performance due to the manufacturing variability, it has been shown that the use of 3D printers is feasible. In this work, an uncertainty analysis is presented for the band gaps of beams with periodically distributed resonators manufactured by 3D printing is proposed. An analytical tool, the WKB (after Wentzel, Kramers and Brillouin) approximation, is used in order to find a suitable generalisation of the wave solutions in slowly varying waveguides and provides a framework for the uncertainty analysis. Material and geometrical variability are modelled as spatially correlated randomness and the statistics of the forced response are derived.

1 Introduction

Periodic structures can be designed to exhibit elastic band gap behaviour by varying material or geometrical properties to present a Bragg scattering effect, i.e. phononic crystals. Other examples include periodically distributed resonators, or inclusions that can be designed to be in the sub-Bragg region, i.e. acoustic metamaterials. These structures have various applications in passive noise and vibration control through elastic stop bands [1–5], where only non-propagating (evanescent) waves are generated. A straight beam with periodically attached resonators works like a local resonant metamaterial, which has a stop band around the tuned natural frequency of the resonators that is associated to a vibration attenuation zone. The beam and resonator coupling is the mechanism responsible to produce the band gap in this case [6, 7]. In addition, an acoustic mode can be observed at low-frequencies where the beam and the resonators move in-phase and an optical mode at higher-frequencies where the beam and the resonators move out-of-phase.

Recently, additive manufacturing and its developments have enabled the production of mechanical structures with complex geometry at a low cost [8], becoming an emerging topic in phononic crystals and metamaterials [9]. Like any manufacturing process, it can introduce variability in the material and geometrical properties of the unit cells [10], affecting the band gap performance and consequently the vibration attenuation [11]. Wave-based methods commonly assume that waveguide properties are homogeneous, thus limiting the application of such approaches to the investigation of the influence of manufacturing variability on the band gaps behaviours. This assumption arises mainly because analytical

solutions for non-homogeneous waveguides are only possible for very particular cases, for example acoustic horns, ducts, rods and beams, e.g. [12–15].

The Spectral Element Method (SEM) [16, 17], is a wave-based method relying on the exact analytical solution to generate dynamic stiffness matrices, and it is often employed in the dynamic analysis of periodic structures. Moreover, by modelling only one periodic unit cell, it is possible to assess free wave propagation through dispersion curves as well as the forced response in the frequency and time domains. This approach is, however, limited to homogeneous or piecewise constant waveguides. Non-homogeneous waveguides can be modelled with SEM by dividing the structures into a number of elements, but making the method less appealing in terms of computation cost. This is an important factor to take into account especially when considering randomly varying material and geometric properties, in which the calculation of the response statistics usually involves a great number of evaluations over a large frequency band.

The classical WKB approximation is a method for finding suitable modifications of plane-wave solutions for non-homogeneous waveguides [18]. Named after Wentzel, Kramers and Brillouin, it was initially developed for solving the Schrödinger equation in quantum mechanics, and it was also applied to periodic potential function to investigate propagation bands [19]. The formulation assumes that the waveguide properties vary slowly enough such that there are no or negligible reflections due to these local changes, even if the net change is large, and it can be extended to include spatially correlated random variability [20]. It maintains the wave-like interpretation of non-uniform waveguides, but it is restricted to available analytical solutions. Fabro et al. [21] have proposed an approach to extend the applicability of the WKB using a finite element approach, so that no analytical solution is required.

In this work, the WKB approximation is used along with the SEM in order to find a suitable generalization of the wave solutions considering slowly varying properties of a beam with periodically attached resonators. This approach provides a framework to represent randomness with spatial correlation of the periodic unit cell and then to quantify the effects of this uncertainty in band gaps. Section 2 presents the dynamic model of the nominal period unit cell using the SEM. A dynamic stiffness matrix is assembled using Timoshenko frame spectral elements [17] for the I-beam and the resonators and it is used to create a transfer matrix, from which the wave properties can calculated as a function of the position along the waveguide. In Section 3, this information is used with the WKB approach. The phase change is calculated using a Gauss-Legendre quadrature scheme for numerical integration of the local wavenumber. At each integration point, the SEM is used to calculate the wavenumber. These points are kept to a minimum to reduce computation cost while being able to capture the non-homogeneity to a given accuracy. The wave amplitude change is calculated using conservation of power.

This work aims at investigating the effects of the random variability due to the additive manufacturing process on the performance of the elastic band gap behaviour in creating a stop band effect on the forced response of the waveguide. A numerical example considers the spatially varying Young's modulus, aiming to represent the effects of the random variability due to the additive manufacturing process on the performance of the elastic band gap behaviour in creating a stop band effect on the forced response of the waveguide. The effects of the variability of the others material and geometrical properties can be evaluated using the same approach. Random field properties are expressed in terms of a Karhunen-Loeve (KL) expansion using an analytical solution for a specific family of correlation functions [22]. The forced response at one end to a point excitation at the other end is calculated and results show good agreement when compared to the direct inversion of the dynamic stiffness matrix obtained from assembling the SEM elements. They require only a few SEM evaluations. It is also shown that variability in the Young's modulus of the I-beam does not affect the performance of the band gap, while variability of the stiffness of the resonator can drastically reduce the band gap performance. In addition, it is also shown that the correlation length plays a significant role on the band gap region.

2 Dynamic modelling using the spectral element approach

The unit cell, an I-beam with attached resonators on both sides of the web, was built using Timoshenko frame spectral elements (SE) [16, 17]. These elements have two nodes and six degrees of freedom (DOF)

per node, three displacements and three rotations, which describe vertical bending, lateral bending, extension/compression and torsion dynamic effects. The main I-beam is composed of three nodes (1-3) with resonators placed in the middle node (2). The side resonators are composed of two elements, one characterized by stiffness (nodes 2-4 and 2-6) and the other by mass (nodes 4-5 and 6-7). The coupling between the I-beam and the resonators is responsible for the band gaps in the dispersion relation and corresponding attenuation zones in the frequency response of the built up structure [11]. After the assembly process, the dynamic stiffness matrix of the periodic unit cell can be partitioned as

$$\begin{bmatrix} \mathbf{D_{LL}} & \mathbf{D_{LI}} & \mathbf{D_{LR}} \\ \mathbf{D_{IL}} & \mathbf{D_{II}} & \mathbf{D_{IR}} \\ \mathbf{D_{RL}} & \mathbf{D_{RI}} & \mathbf{D_{RR}} \end{bmatrix} \mathbf{q} = \mathbf{f}, \tag{1}$$

where *I*, *L* and *R* are related to interior, left and right DOF, respectively, and $\mathbf{q}$ and $\mathbf{f}$ are vectors of nodal DOF and external forces, respectively. If no forces are applied to the interior DOFs, Eq. (1) can be written as a function of the *L* and *R* DOFs using dynamic condensation, leading to $\mathbf{D}^*_{\boldsymbol{BB}} = \mathbf{D_{BB}} - \mathbf{D_{BI}}(\mathbf{D_{II}})^{-1}\mathbf{D_{IB}}$, where the sub index *B* can be replaced by *L* or *R* [23, 24].

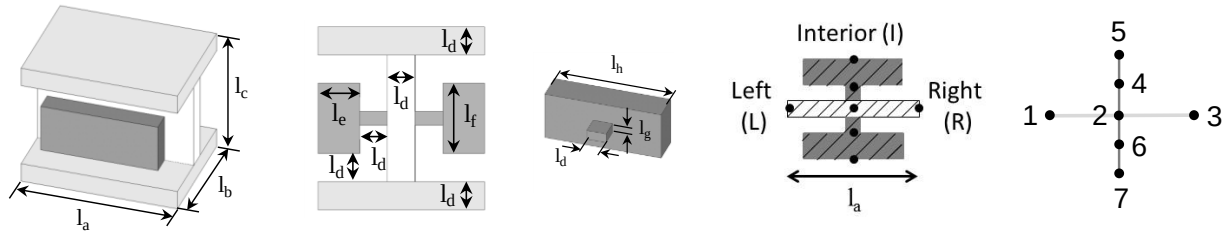

(a) (b) (c) (d) (e)

Figure 1: Schematics of the unit cell in isometric view (a), cross-section view (b), resonator details (c), neutral plane view with left, right and interior nodes (d) and corresponding representation using SE (e).

Considering the relations between internal and external forces, the state vector of the left-hand side cross section can be related to the right-hand side one by a transfer matrix, which is written in terms of the condensed dynamic transfer matrix as

$$\begin{bmatrix} \mathbf{q_R} \\ \mathbf{f_R} \end{bmatrix} = \begin{bmatrix} -\mathbf{D^*_{LR}}^{-1}\mathbf{D^*_{LL}} & \mathbf{D^*_{LR}}^{-1} \\ -\mathbf{D^*_{RL}} + \mathbf{D^*_{RR}}\mathbf{D^*_{LR}}^{-1}\mathbf{D^*_{LL}} & -\mathbf{D^*_{RR}}\mathbf{D^*_{LR}}^{-1} \end{bmatrix} \begin{bmatrix} \mathbf{q_L} \\ \mathbf{f_L} \end{bmatrix} \text{ or } \begin{bmatrix} \mathbf{q_R} \\ \mathbf{f_R} \end{bmatrix} = \mathbf{T} \begin{bmatrix} \mathbf{q_L} \\ \mathbf{f_L} \end{bmatrix}. \tag{2}$$

In addition, by using the Bloch's theorem, the state vector of the left cross-section is related to the one of the right cross-section by means of the eigenvalues of $\mathbf{T}$, $[\mathbf{q}_R^T \quad \mathbf{f}_R^T]^T = \mu[\mathbf{q}_L^T \quad -\mathbf{f}_L^T]^T$, which are functions of the j^{th} wavenumbers k_j, with $\mu_j = e^{-ik_j l_a}$. Replacing this relation in Eq. (2), yields the following eigenvalue problem

$$\mathbf{T}\boldsymbol{\phi}_j = \mu_j \boldsymbol{\phi}_j \tag{3}$$

This eigenproblem provides 2*n* eigenvalues and the respective eigenvectors, where *n* corresponds to the number of DOFs associated with each cross section. While the eigenvalues are associated with phase change or attenuation along the beam length, the eigenvectors, or wave mode shapes, indicate the spatial distribution of the displacements and forces on the cross section [23, 24]. They appear in pairs $(\mu_j, \boldsymbol{\phi}_j^+)$ and $(1/\mu_j, \boldsymbol{\phi}_j^-)$ corresponding to *n* positive and negative going travelling waves, respectively.

The eigenvectors can be rearranged such that $\boldsymbol{\phi}^+ = \begin{bmatrix} \boldsymbol{\phi}_q^+ \\ \boldsymbol{\phi}_f^+ \end{bmatrix}$ and $\boldsymbol{\phi}^- = \begin{bmatrix} \boldsymbol{\phi}_q^- \\ \boldsymbol{\phi}_f^- \end{bmatrix}$ and are then used for a linear transformation of the displacement and force from the wave domain to the physical domain

$$\mathbf{q_L} = \boldsymbol{\phi}_\mathbf{q}^+\mathbf{a}^+ + \boldsymbol{\phi}_\mathbf{q}^-\mathbf{a}^- \text{ and } \mathbf{f_L} = \boldsymbol{\phi}_\mathbf{f}^+\mathbf{a}^+ + \boldsymbol{\phi}_\mathbf{f}^-\mathbf{a}^-, \tag{4}$$

where $\mathbf{a}^+$ and $\mathbf{a}^-$ are respectively positive-going and negative-going wave amplitudes. Any boundary condition can subsequently be written as $\mathbf{Af} + \mathbf{Bq} = \mathbf{0}$, so that the reflection matrices are given by [15, 25]

$$\boldsymbol{\Gamma}_\mathbf{L} = -\left(\mathbf{A}\boldsymbol{\phi}_\mathbf{f}^+ + \mathbf{B}\boldsymbol{\phi}_\mathbf{q}^+\right)^{-1}\left(\mathbf{A}\boldsymbol{\phi}_\mathbf{f}^- + \mathbf{B}\boldsymbol{\phi}_\mathbf{q}^-\right) \text{ and } \boldsymbol{\Gamma}_\mathbf{R} = -\left(\mathbf{A}\boldsymbol{\phi}_\mathbf{f}^- + \mathbf{B}\boldsymbol{\phi}_\mathbf{q}^-\right)^{-1}\left(\mathbf{A}\boldsymbol{\phi}_\mathbf{f}^+ + \mathbf{B}\boldsymbol{\phi}_\mathbf{q}^+\right), \tag{5}$$

In this work, it is particularly interesting to calculate the time averaged power transmitted through the cross-section, i.e.

$$P = -\frac{1}{2}\mathrm{Re}\{i\omega\mathbf{f}^H\mathbf{q}\} = \frac{\omega}{2}\mathrm{Im}\{\mathbf{f}^H\mathbf{q}\}, \tag{6}$$

where the superscript H stands for the Hermitian.

The forced response can be calculated using the global dynamic stiffness matrix, assembled by the usual finite or spectral element method procedure. Once the boundary conditions have been applied, the corresponding displacements can be calculated by direct inversion. Alternatively, the wave modes and wavenumbers obtained from the unit cell can also be used to calculate the forced response in terms of propagating and reflection matrices. This approach is suitable for use within the WKB approximation and it is detailed in the next section.

3 The WKB approximation using the spectral element approach

The WKB formulation has been applied in many fields of engineering, including, acoustics [26, 27] and structural dynamics [18, 20, 28]. However, the WKB approximation breaks down if the properties change rapidly or when the travelling wave reaches a local cut-off section where the wave mode ceases to propagate. This transition, also known as a turning point, leads to an internal reflection, breaking down the main assumption in the theory, requiring a different approximation for certain frequency bands (e.g. [29]). Assuming a time harmonic solution, $u(x,t) = U(x)\, e^{-i\omega t}$, it is possible to define a local wavenumber $k(x)$. Thus, the *eikonal* function $S(x) = \ln \widetilde{U}(x) + i\theta(x)$ is introduced, in order to find wave solutions of the kind [30]

$$U(x) = e^{S(x)} = \widetilde{U}(x)e^{\pm i\theta(x)}. \tag{7}$$

It is possible to define positive $\mathbf{b}^+ = \boldsymbol{\Lambda}^+(x_a, x_b)\mathbf{a}^+$ and negative going $\mathbf{b}^- = \boldsymbol{\Lambda}^-(x_a, x_b)\mathbf{a}^-$ propagation matrices for a wave travelling between x_a and x_b, with $x_b = x_a + nl_a$, where n is an integer number. This condition is necessary due to the periodic condition of the unit cell, then the propagation matrices can be indexed to the cell number as $\boldsymbol{\Lambda}^+(x_a, x_b) = \boldsymbol{\Lambda}^+(0, n)$ and $\boldsymbol{\Lambda}^-(x_a, x_b) = \boldsymbol{\Lambda}^-(0, n)$. In this work, the forced response can be considered as in Fig. 2, where the wave amplitudes are given at the excitation point by

$$\mathbf{c}^+ = \mathbf{e}^+ + \mathbf{a}^+, \tag{8}$$

where $\mathbf{e}^+$ is the amplitude of the waves directly generated from the excitation that can be calculated from equilibrium and continuity conditions, by solving [15]

$$\boldsymbol{\phi}_f^+\mathbf{e}^+ = \mathbf{f}_\mathbf{ext}, \tag{9}$$

either by direct inversion or by using the orthogonality properties of the left eigenvector of the transfer matrix. Wave amplitudes at the boundaries are related by the reflection matrices as $\mathbf{a}^+ = \boldsymbol{\Gamma}_L\mathbf{a}^-$ and $\mathbf{b}^- = \boldsymbol{\Gamma}_R\mathbf{b}^+$. The travelling wave amplitudes are related by the propagating matrices as $\mathbf{b}^+ = \boldsymbol{\Lambda}^+(0,n)\mathbf{a}^+$ and $\mathbf{b}^- = \boldsymbol{\Lambda}^-(0,n)\mathbf{a}^-$. These relations can be used to find

$$\mathbf{b}^+ = [\mathbf{I} - \boldsymbol{\Lambda}^+(0,n)\boldsymbol{\Gamma}_L\boldsymbol{\Lambda}^-(0,n)\boldsymbol{\Gamma}_R]^{-1}[\boldsymbol{\Lambda}^+(0,n)\mathbf{e}^+], \tag{10}$$

from which the input mobility can be calculated. The same rationale can be used to calculate the response at any point in the waveguide [25]. The propagation matrices are given by [21]

$$\boldsymbol{\Lambda}^+(0,n) = diag\left\{exp\left[-i\theta_j(0,n) + \gamma_j(0,n)\right]\right\}, \tag{11}$$

$$\boldsymbol{\Lambda}^{-}(0,n) = diag\{exp[-i\theta_j(0,n) - \gamma_j(0,n)]\}, \tag{12}$$

where $diag\{\cdot\}$ stands for a diagonal matrix and $\theta_j(0,n)$ is calculated following an integration scheme considering the locally defined wavenumber $k_j^{(n)}$ at the n^{th} cell, and $\gamma_j(0,n)$ is the amplitude change caused by the slowly varying waveguide, Eq. (15). In this work, a numerical integration using a Gauss-Legendre quadrature scheme is applied, *i.e.*

$$\theta_j(x_a, x_b) = \int_{x_a}^{x_b} k_j(x)\, dx \approx \sum_{i=1}^{N_{gl}} G_i k_j(x_i), \tag{13}$$

where G_i are the weights and $k_j(x_i)$ is the j^{th} wavenumber calculated from the unit cell dynamic model at the sampling point x_i, defined by the Gauss-Legendre quadrature. The proprieties are evaluated at x_i from a given function describing the spatial variability and then assumed constant within the unit cell. This is equivalent to a mid-point discretization for the spatial variability given by a random field, [31–33]. The integration scheme gives the exact integral for a polynomial of a given order depending on the number of points N_{gl}. Therefore, this is equivalent to a polynomial fitting of the wavenumber over the waveguide between x_a and x_b. The number of points used by the quadrature must be kept to a minimum number of evaluations, to avoid excessive computational cost. No re-meshing of the model is necessary for each evaluation.

The amplitude change can be calculated from the energy conserving property as a consequence of the WKB approximation [18, 34]. Therefore, for a positive-going wave travelling from x_a, with amplitude a^+, to $x_b = x_a + nl_a$, with amplitude b^+, assuming no damping, the time average power transmitted through the cross-section at both positions must be equal, leading to

$$\left|a_j^+\right|^2 Re\{i\omega \boldsymbol{\phi}_{f,j}^{+H}(0)\boldsymbol{\phi}_{q,j}^{+}(0)\} = \left|b_j^+\right|^2 Re\{i\omega \boldsymbol{\phi}_{f,j}^{+H}(n)\boldsymbol{\phi}_{q,j}^{+}(n)\}. \tag{14}$$

This relation is written in order to define the amplitude change, giving

$$\gamma_j(0,n) = log\left(\frac{|b^+|}{|a^+|}\right) = \frac{1}{2} log\left(\frac{Re\{i\omega \boldsymbol{\phi}_{f,j}^{H}(0)\boldsymbol{\phi}_{q,j}(0)\}}{Re\{i\omega \boldsymbol{\phi}_{f,j}^{H}(n)\boldsymbol{\phi}_{q,j}(n)\}}\right). \tag{15}$$

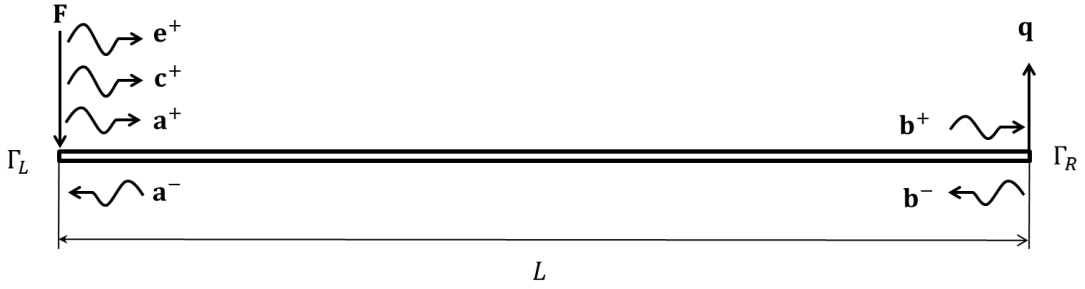

Figure 2: Point excitation and wave amplitudes on a waveguide with slowly varying properties. The displacement and force from the wave domain to the physical domain.

4 Random variability

Random field theory can be used to model spatially distributed randomness using a probability measure. There are a number of methods available in the literature for generating random fields [22, 32, 33, 35], including formulations using series expansions that are able to represent the field using deterministic spatial functions and random uncorrelated variables. The KL expansion is a special case where these deterministic spatial functions are orthogonal and derived from the covariance function.

A Gaussian homogeneous random field $H(x,p)$ with a finite, symmetric and positive definite covariance function $C_H(x_1,x_2)$, defined over a domain D, has a spectral decomposition in a generalized series as [22]

$$H(x) = H_0(x) + \sum_{j=1}^{\infty} \sqrt{\lambda_j}\, \xi_j f_j(x), \tag{16}$$

where ξ_j are Gaussian uncorrelated random variables, λ_j and $f_j(x)$ are eigenvalues and eigenfunctions. The eigenvalues and eigenfunctions can be ordered in descending order of eigenvalues and the KL expansion is then calculated with a finite number of terms N_{KL}, chosen by the accuracy of the series in representing the covariance function [36]. As a rule of thumb, N_{KL} can be chosen such that $\lambda_{N_{KL}}/\lambda_1 < 0.1$, and N_{KL} will depend on the correlation length of the random field.

In general, this problem can only be solved numerically by discretizing the covariance function. However, for some families of correlation functions and specific geometries, there exist analytical solutions. One such case is the one dimensional exponentially decaying autocorrelation function, $C(x_1, x_2) = e^{-|x_1 - x_2|/l_c}$, where b is the correlation length, in the interval $-L/2 \leq x \leq L/2$, where L is the length of the domain and where x_1 and x_2 are any two points within the interval. In this case, the KL expansion, for a zero-mean random field, can be written as

$$H(x) = \sum_{j=1}^{N_{kl}} \left[\alpha_j \xi_{1j} \sin(w_{1j} x) + \beta_j \xi_{2j} \cos(w_{2j} x)\right] \tag{17}$$

where ξ_{1j} and ξ_{2j} are Gaussian zero-mean, unity standard-deviation, independent random variables with the properties $\langle \xi_{1j} \rangle = \langle \xi_{1i} \rangle = 0, \langle \xi_{1i} \xi_{2j} \rangle = 0\,, \langle \xi_{1i} \xi_{1j} \rangle = \delta_{ij}$ where $\delta_{ij} = 1$ for $i = j$ and $\delta_{ij} = 0$ for $i \neq j$, and $\alpha_j = \sqrt{\lambda_{1j} / \left(\frac{L}{2} - \frac{\sin(w_{1j} L)}{2 w_{1j}}\right)}$, $\beta_j = \sqrt{\lambda_{2j} / \left(\frac{L}{2} + \frac{\sin(w_{2j} L)}{2 \mathrm{w}_{2\mathrm{j}}}\right)}$, $\lambda_{1\mathrm{j}} = 2c/\left(w_{1i}^2 + c^2\right)$, $\lambda_{2j} = 2c/\left(w_{2i}^2 + c^2\right)$, where $c = 1/b$ and w_{1i} and w_{2i} are the i^{th} roots of the transcendental equations $c \tan w_1 + w_1 = 0$ and $w_2 \tan w_2 - c = 0$, respectively. This expansion is truncated to N_{KL} terms according the weight of the higher order eigenvalues in the series. A complete derivation can be found in the book by Ghanem and Spanos [22].

The KL expansion is then used to describe the Young's modulus of the I-beam and the resonators as a random field in the numerical examples of the following section, given by $E(x) = E_0[1 + \sigma H(x)]$, where E_0 is the nominal value for the Young's modulus and σ is the standard deviation, that can also be seen as a dispersion term quantifying the influence of $H(x)$ on the mean value E_0. The spatial variability is assumed to be constant within each unit cell, using the value of $H(x)$ at its centroid, which is equivalent to the mid-point approach for random field discretization. The slowly varying condition can be achieved by choosing an appropriate value of the correlation length b. The larger the correlation length, the smoother the spatial variability. The Gaussian probability distribution implies that the Young's modulus could assume negative values, but the choice of the parameters makes it a very unlikely event. From a Monte Carlo (MC) sampling framework, the distribution can be clipped to avoid values of Young`s modulus smaller than a given threshold. Even though an analytical solution of the KL expansion is used in this work, the proposed method is not restricted to it and any numerical solution for a different correlation function or probability density function can be directly applied.

5 Numerical examples

In this section some numerical examples are presented aiming to represent the effects of the random variability due to the additive manufacturing process on the performance of the elastic band gap behaviour in creating a stop band effect, i.e. a vibration attenuation zone, on the forced response of the waveguide. The model analysed consists of an I-beam with attached periodic resonators, as described in section 2, with nominal geometric dimensions of the unit cell, shown in Fig. 1, given by $l_a = 16$ mm, $l_b = 12$ mm, $l_c = 13$ mm, $l_d = 2$ mm, $l_e = 3$ mm, $l_f = 5$ mm, $l_g = 1$ mm, and $l_h = 12$ mm. The global structure has 21 cells and is made of polyamide, whose mean properties are shown in Table 1. Only the Young's modulus

of the I-beam and of the periodically attached resonators are considered to be spatially varying, even though it is expected that other material and geometric properties are also affected by the additive manufacturing process. The WKB approximation using the spectral element approach, as described in section 3, is used to calculate the forced response and results are compared to the direct inversion of the dynamic stiffness matrix. The phase change integral, Eq. (13), was performed using $N_{gl} = 8$ points. Even though the latter approach produces smaller matrices when compared to the usual finite element approach, it does not benefit from the periodicity of the structure.

	I-beam	**Resonator mass**	**Resonator spring**
Young's modulus (GPa)	0.86	0.86	0.72
Density (kg/m^3)	700	1000	700
Poisson coefficient	0.39	0.39	0.39
Structural damping ratio	0.03	0.03	0.03

Table 1: Polyamide nominal material properties used in the SEM model.

Figure 3 presents the real and imaginary parts of the dispersion curve of the nominal periodic unit cell for all of the wave modes present in the waveguide, normalized by the cell length l_a. It can be noticed the band gap behaviour in the frequency band between 800 Hz and 1200 Hz is related to the flexural resonators vertical natural frequencies, as shown in Table 2 [11]. Figures 4 and 5 present the forced response considering the spatially varying Young's modulus in the I-beam only and in the periodically attached resonators only, respectively. The Young's modulus value is given by Eq. (16), for both cases with $\sigma = 0.1$ and correlation length $b = 0.4\,L$ and $b = L$. For this first analysis, only one sample of the KL expansion is used, i.e. it is a deterministic analysis, but with changing properties from one unit cell to another. A very good agreement between the WKB the full SEM approaches. It can be noticed that the variability in the material properties of the I-beam affects only the FRF away from band gap region, but variability in the stiffness of the resonators greatly affects the band gap performance, in terms of vibration attenuation, 50 dB reduction, and also in terms of frequency band. Despite the great reduction in performance, it is still feasible for applications on vibration attenuation.

The uncertainty analysis is carried out using a Monte Carlo sampling scheme, with 250 samples, which is enough to achieve acceptable convergence. Firstly, randomness is considered only in the Young's modulus of the I-beam for two cases of correlation length, $b = 0.4\,L$ and $b = L$. Figure. 6 presents the 95% confidence bounds of the forced response and mean value obtained from the WKB approach and full SEM model. Results are compared with the forced response obtained from the nominal waveguide, and it can be noticed that it does not introduce uncertainty in the band gap region, regardless of the correlation length. However, when the variability is considered only in the stiffness properties of the resonators, as shown in Fig. 7, it can be seen that the performance of the band gap is greatly affected, as expected from the results obtained in the deterministic analysis. The lower confidence bounds of the forced response reached a performance almost as good as the nominal case, which means that there are some configurations that are almost as good as the nominal periodic conditions in producing the band gaps. The upper confidence bound show that there is a high probability of reaching feasible levels of attenuation in the band gap frequency band, and that this probability is higher for the lower correlation length.

	Torsion	**Vertical Flexural**	**Lateral Flexural**
Frequency (Hz)	776.7	941.6	1315.4

Table 2: Natural frequencies related to the torsion, vertical and lateral flexural mode shapes of the resonator.

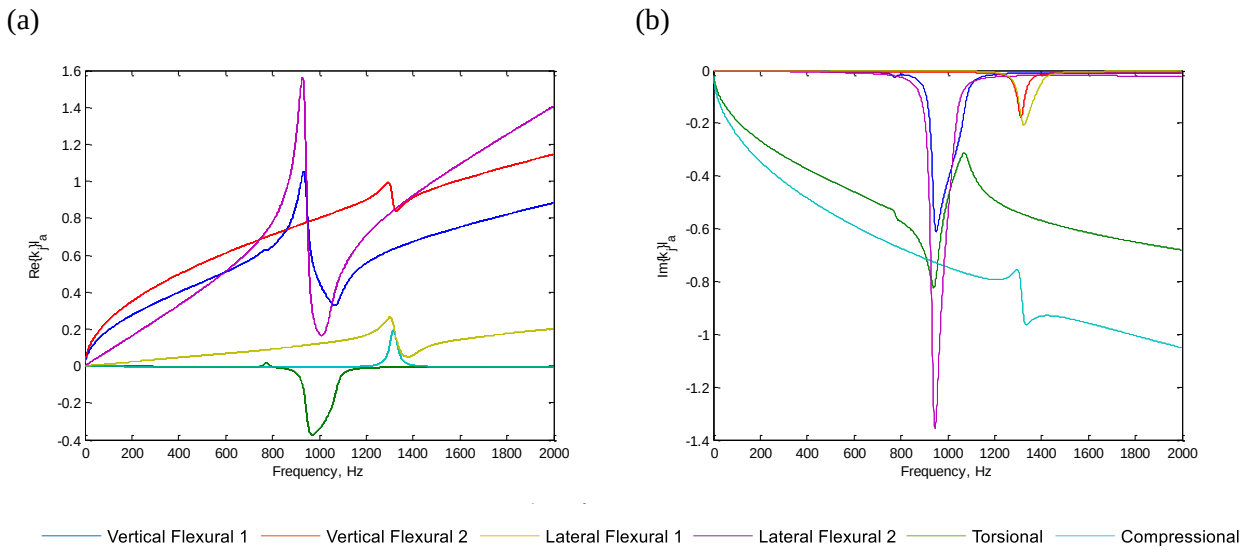

Figure 3: Real (a) and imaginary (b) parts of the dispersion curves of the beam with identical periodically distributed resonators.

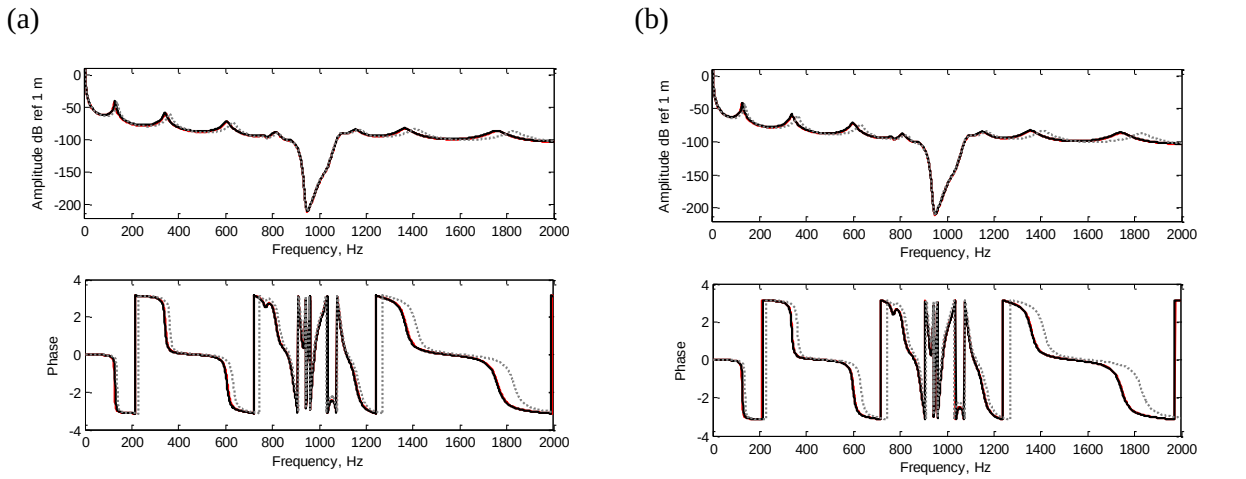

Figure 4: Forced response from full SEM model (red) and the WKB approach (black) considering one sample of random Young's modulus for the I-beam with $\sigma = 0.1$ and (a) $b = 0.4L$ and b) $b = L$ correlation length, and using nominal periodic properties (grey dotted).

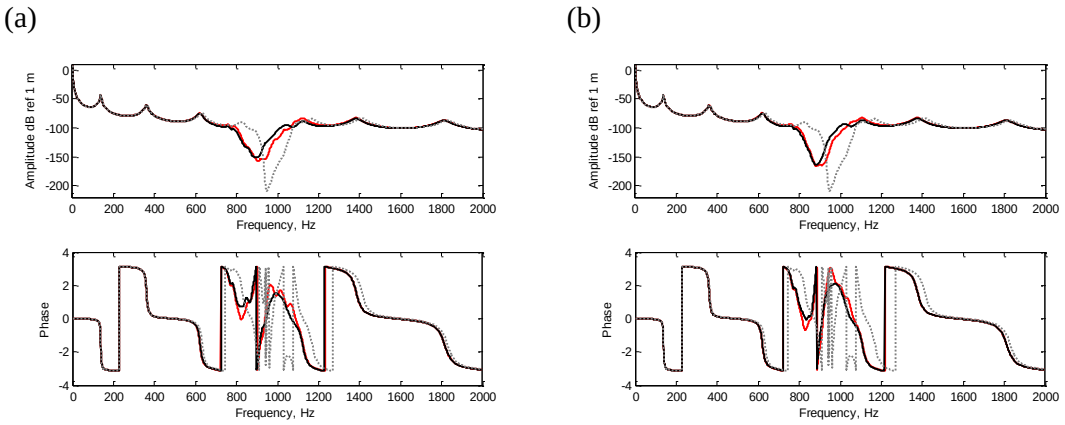

Figure 5: Forced response from full SEM model (red) and the WKB approach (black) considering one sample of random Young's modulus for the resonators with $\sigma = 0.1$ and (a) $b = 0.4L$ and (b) $b = L$ correlation length, and using nominal periodic properties (grey dotted).

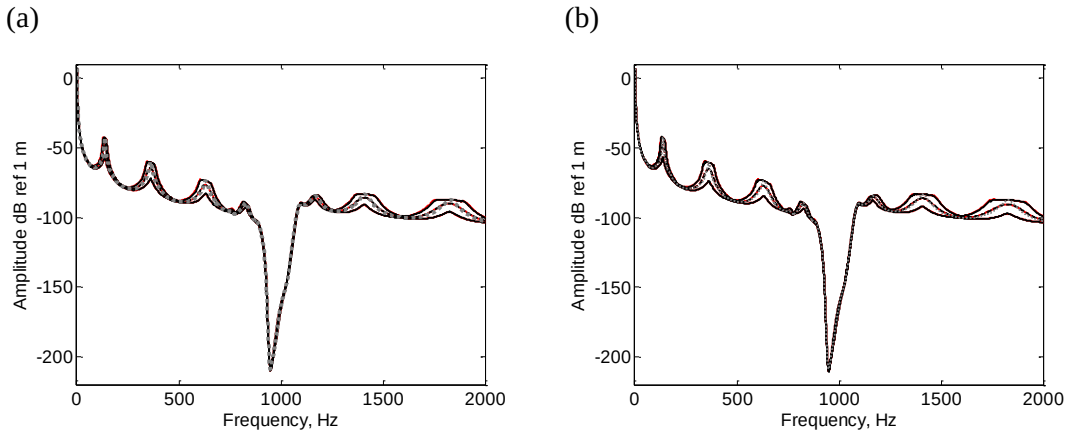

Figure 6: Forced response 95% confidence bounds (full line) and mean value (dashed) from full SEM model (red) and the WKB approach (black) considering random Young's modulus for the I-beam with $\sigma = 0.1$ and (a) $b = 0.4L$ and (b) $b = L$ correlation length, and using nominal periodic properties (grey dotted).

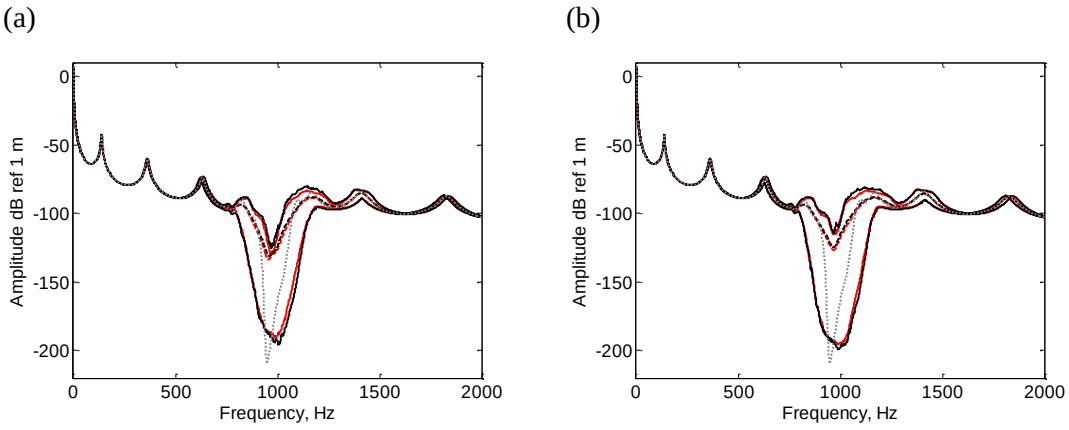

Figure 7: Forced response 95% confidence bounds (full line) and mean value (dashed) from full SEM model (red) and the WKB approach (black) considering random Young's modulus for the resonators with $\sigma = 0.1$ and (a) $b = 0.4L$ and (b) $b = L$ correlation length, and using nominal periodic properties (blue dotted).

6 Concluding remarks

A method was proposed for uncertainty analysis of beams with periodically attached resonators produced from additive manufacturing, or 3D printing. The WKB approximation is used along with the SEM in order to find a suitable generalization of the wave solutions considering slowly varying properties of the beam with periodically attached resonators. It extends the applicability of the WKB approach to cases where no analytical solution exists by using the SEM. This approach provides a framework to represent randomness with spatial correlation of the periodic unit cell and then to quantify the effects of this uncertainty in the band gaps. Properties within the unit cell were considered as constant. A Gaussian random field and an analytical solution of the KL expansion were used to model the spatially correlated variability, but different random field models, including numerical solutions, can be used straightforwardly.

It was shown that only variability in the material properties of resonators affects the performance of the vibration attenuation in the band gap region. The maximum attenuation is greatly reduced, but it is still feasible for vibration isolation applications. It was also shown that the correlation length of the spatial variability also plays a role. Variability in the material properties of the host I-beam only affects the forced response away from the band gap region. Understanding these influences is fundamental for the control of manufacturing tolerances, such that a minimum performance of the band gap is guaranteed.

Further possible steps to investigate include analysing the influence of the other material and geometrical properties and comparison of the simulations with experimental results.

Acknowledgements

The authors gratefully acknowledge the financial support of the Brazilian National Council of Research (CNPq) Process number 445773/2014-6, the Federal District Research Foundation (FAPDF) Process number 0193001040/2015, the São Paulo Research Foundation (FAPESP) Process number 2014/19054-6 and 2015/15718-0 and the Royal Society for the Newton International Exchanges Fund reference number IE140616.

References

[1] T. L. Huang, M. N. Ichchou, O. A. Bareille, M. Collet, M. Ouisse, *Traveling wave control in thin-walled structures through shunted piezoelectric patches*, Mechanical Systems and Signal Processing, Vol. 39, No. 1–2, pp. 59–79, (2013).

[2] M. I. Hussein, M. J. Leamy, M. Ruzzene, *Dynamics of Phononic Materials and Structures: Historical Origins, Recent Progress, and Future Outlook*, Applied Mechanics Reviews, Vol. 66, No. 4, pp. 040802–040802, (2014).

[3] Y. Fan, M. Collet, M. Ichchou, L. Li, O. Bareille, Z. Dimitrijevic, *A wave-based design of semi-active piezoelectric composites for broadband vibration control*, Smart Materials and Structures, Vol. 25, No. 5, p. 55032, (2016).

[4] H. Sun, X. Du, P. F. Pai, *Theory of Metamaterial Beams for Broadband Vibration Absorption*, Journal of Intelligent Material Systems and Structures, (2010).

[5] P. F. Pai, *Metamaterial-based Broadband Elastic Wave Absorber*, Journal of Intelligent Material Systems and Structures, Vol. 21, No. 5, pp. 517–528, (2010).

[6] Y. Xiao, J. Wen, D. Yu, X. Wen, *Flexural wave propagation in beams with periodically attached vibration absorbers: Band-gap behavior and band formation mechanisms*, Journal of Sound and Vibration, Vol. 332, No. 4, pp. 867–893, (2013).

[7] M Ruzzene, *Internally Resonating Metamaterials for Wave and Vibration Control*, in *Proceedings of the Noise and Vibration - Emerging Technologies*, Dubrovnik, Croatia, (2015), p. FORUMIII3-1-26.

[8] R. Hague, I. Campbell, P. Dickens, *Implications on design of rapid manufacturing*, Proceedings of the Institution of Mechanical Engineers, Part C: Journal of Mechanical Engineering Science, Vol. 217, No. 1, pp. 25–30, (2003).
[9] S. A. Cummer, J. Christensen, A. Alù, *Controlling sound with acoustic metamaterials*, Nature Reviews Materials, Vol. 1, No. 3, p. 16001, (2016).
[10] B. P. Bernard, B. A. M. Owens, B. P. Mann, *Uncertainty Propagation in the Band Gap Structure of a 1D Array of Magnetically Coupled Oscillators*, Journal of Vibration and Acoustics, Vol. 135, No. 4, pp. 041005–041005, (2013).
[11] D Beli, J R F Arruda, *Influence of additive manufacturing variability in elastic band gaps of beams with periodically distributed resonators*, in *Proceedings of the 3rd International Symposium on Uncertainty Quantification and Stochastic Modeling*, Maresias, Brazil, (2016).
[12] Q. S. Li, *Exact solutions for free longitudinal vibrations of non-uniform rods*, Journal of Sound and Vibration, Vol. 234, pp. 1–19, (2000).
[13] M. Eisenberger, *Exact longitudinal vibration frequencies of a variable cross-section rod*, Applied Acoustics, Vol. 34, pp. 123–130, (1991).
[14] S. Guo, S. Yang, *Wave motions in non-uniform one-dimensional waveguides*, Journal of Vibration and Control, Vol. 18, pp. 92–100, (2012).
[15] S. K. Lee, B. R. Mace, M. J. Brennan, *Wave propagation, reflection and transmission in non-uniform one-dimensional waveguides*, Journal of Sound and Vibration, Vol. 304, pp. 31–49, (2007).
[16] J. F. Doyle, *Wave Propagation in Structures*. New York: Springer, (1997).
[17] U. Lee, *Spectral Element Method in Structural Dynamics*. Singapore: John Wiley & Sons, (2009).
[18] A. D. Pierce, *Physical interpretation of the WKB or eikonal approximation for waves and vibrations in inhomogeneous beams and plates*, The Journal of the Acoustical Society of America, Vol. 48, pp. 275–284, (1970).
[19] N. L. Balazs, *One dimensional band theory in the WKB approximation*, Annals of Physics, Vol. 53, No. 3, pp. 421–438, (1969).
[20] A. T. Fabro, N. S. Ferguson, T. Jain, R. Halkyard, B. R. Mace, *Wave propagation in one-dimensional waveguides with slowly varying random spatially correlated variability*, Journal of Sound and Vibration, Vol. 343, pp. 20–48, (2015).
[21] A. Fabro, N. Ferguson, B. Mace, *Wave propagation in slowly varying one-dimensional random waveguides using a finite element approach*, in *Proceeding of the 3rd International Symposium on Uncertainty Quantification and Stochastic Modeling*, Maresias, Brazil, (2016).
[22] R. Ghanem, P. D. Spanos, *Stochastic Finite Elements: A Spectral Approach*, Revised edition. Minneola, N.Y.: Dover Publications, (2012).
[23] B. R. Mace, D. Duhamel, M. J. Brennan, L. Hinke, *Finite element prediction of wave motion in structural waveguides*, The Journal of the Acoustical Society of America, Vol. 117, No. 5, pp. 2835–2843, (2005).
[24] J.-M. Mencik, *A wave finite element-based formulation for computing the forced response of structures involving rectangular flat shells*, International Journal for Numerical Methods in Engineering, Vol. 95, No. 2, pp. 91–120, (2013).
[25] J. M. Renno, B. R. Mace, *On the forced response of waveguides using the wave and finite element method*, Journal of Sound and Vibration, Vol. 329, pp. 5474–5488, (2010).
[26] S. W. Rienstra, *Sound propagation in slowly varying lined flow ducts of arbitrary cross-section*, Journal of Fluid Mechanics, Vol. 495, pp. 157–173, (2003).
[27] J. P. Arenas, M. J. Crocker, *A note on a WKB application to a duct of varying cross-section*, Applied Mathematics Letters, Vol. 14, pp. 667–671, (2001).
[28] R. D. Firouz-Abadi, H. Haddadpour, A. B. Novinzadeh, *An asymptotic solution to transverse free vibrations of variable-section beams*, Journal of Sound and Vibration, Vol. 304, pp. 530–540, (2007).
[29] A. H. Nayfeh, *Perturbation methods*. New York: Wiley, (1973).
[30] G. B. Whitham, *Linear and nonlinear waves*. New York: John Wiley & Sons, (1974).
[31] A. Der Kiureghian, J.-B. Ke, *The stochastic finite element method in structural reliability*, Probabilistic Engineering Mechanics, Vol. 3, pp. 83–91, (1988).
[32] G. Stefanou, *The stochastic finite element method: Past, present and future*, Computer Methods in Applied Mechanics and Engineering, Vol. 198, pp. 1031–1051, (2009).

[33] B. Sudret, A. Der Kiuereghian, *Stochastic Finite Element methods and reliability: A state-of-Art report*, University of California, Berkeley, UCB/SEMM-2000/08, (2000).
[34] R. Nielsen, S. Sorokin, *The WKB approximation for analysis of wave propagation in curved rods of slowly varying diameter*, Proc. R. Soc. A, Vol. 470, No. 2167, p. 20130718, (2014).
[35] E. Vanmarcke, *Random Field: Analysis and Synthesis*, 2nd Revised and Expanded. Cambridge, MA: Word Scientific, (2010).
[36] S. P. Huang, S. T. Quek, K. K. Phoon, *Convergence study of the truncated Karhunen–Loeve expansion for simulation of stochastic processes*, International Journal for Numerical Methods in Engineering, Vol. 52, pp. 1029–1043, (2001).